12-8-2011

Ferromagnetic ZnO Nanocrystals and Al-induced Defects

Chinmay Phadnis
University of Pune

Darshana Y. Inamdar
University of Pune

Igor Dubenko
Southern Illinois University Carbondale

Arjun K. Pathak
Southern Illinois University Carbondale

Naushad Ali
Southern Illinois University Carbondale

See next page for additional authors

Published in *Journal of Applied Physics*, Vol. 110 No. 11 (2011) at doi: 10.1063/1.3665637

Ferromagnetic ZnO nanocrystals and Al-induced defects

Chinmay Phadnis,[1] Darshana Y. Inamdar,[1] Igor Dubenko,[2] Arjun Pathak,[2] Naushad Ali,[2] and Shailaja Mahamuni[1,a)]
[1]*Department of Physics, University of Pune, Pune 411 007, India*
[2]*Department of Physics, Southern Illinois University Carbondale, Illinois 62901, USA*

(Received 18 October 2010; accepted 8 November 2011; published online 8 December 2011)

ZnO nanocrystals (NCs) capped with polyvinyl pyrrolidone reveal room temperature ferromagnetism. Incorporation of Al^{3+}-ions induce defects in ZnO NCs leading to quenching of excitonic luminescence of ZnO at the cost of an increase in the intensity of oxygen vacancy related emission. Photoluminescence excitation spectra exhibit an additional hump like feature attributed to Al-doping. Saturation magnetization of Al^{3+}-doped ZnO NCs is the same as that of the undoped ZnO NCs. However, a remarkable decrease in the coercivity associated with change in the nature of M (T) curve and electron paramagnetic resonance signal with $g = 1.96$ is observed consequent to Al doping. The results provide direct evidence of the defects within the core of NCs that are responsible for the ferromagnetic ordering in the Al^{3+}-doped ZnO. The M(T) curve unravels a typical exchange mechanism. © *2011 American Institute of Physics*. [doi:10.1063/1.3665637]

I. INTRODUCTION

Recent observations compel one to infer that the ferromagnetism does not rely exclusively on the localized moments in magnetic ions, but can also be leading to magnetic moments generated[1,2] due to the defects. These studies opened exciting topic for research coined as "d^0 ferromagnetism." In particular, nanocrystals (NCs) having large surface to volume ratio are attractive candidates to study d^0 ferromagnetism. It is believed that defects located at the interface of NC and the capping agent are responsible for ferromagnetism.[3–8] Efforts are underway to prepare different types of nanocrystalline ferromagnets as well as to understand the nature of defects responsible.[9–12] Earlier, we had reported[10] ZnO NCs to be ferromagnetic at room temperature. Ferromagnetism observed[3] in thermally annealed ZnO NCs is attributed to the oxygen vacancy clusters. Others proposed room temperature ferromagnetism (RTFM) to be associated with holes in the *d* shell due to charge transfer[5–8] from the Zn atom at the surface to the capping agent. In case of doped ZnO NCs, it is usually believed[9–11] that dopant induced defects contribute to RTFM. In spite of the considerable efforts undertaken to understand the optical and magnetic properties of the d^0 ferromagnetic materials, the detailed underlying mechanism is still not clear. Compared to the conventional diluted magnetic semiconductors, one obvious advantage of d^0 ferromagnetism is that clusters or secondary phases formed by the dopant do not contribute to magnetism.[12]

Al^{3+}-doped ZnO would be suitable to study such d^0 ferromagnetism in NCs, as secondary phase even if present (which is elusive to the available probes) will not be magnetic. Secondly, Al^{3+} in ZnO acts as a donor. And ionic size of Al^{3+}-ion being smaller than Zn^{2+}-ion, it occupies substitutional position without distorting the lattice. Earlier studies indicated[13] increase in charge carrier concentration in Al^{3+}-doped ZnO NCs. Ferromagnetism in wide bandgap material such as ZnO is observed[14] to disappear at critical charge carrier density. The case of Al^{3+}-doped ZnO NCs allows one to examine this hypothesis in nanocrystalline regime. Further, in the present work, defects responsible for ferromagnetic ordering in ZnO NCs are identified using electron paramagnetic resonance (EPR) spectroscopy.

Here, we describe the optical and magnetic properties of undoped as well as Al^{3+}-doped ZnO NCs. Undoped ZnO NCs capped with polyvinyl pyrrolidone (PVP) are ferromagnetic at room temperature. Even though oxygen vacancies are present at the surface of ZnO NCs, no signal is observed in EPR. Incorporation of Al^{3+}-ions in ZnO NCs also retain ferromagnetism albeit with substantially reduced coercivity. EPR spectra exhibit monotonic increase in the signal with amount of Al^{3+}-ions in ZnO NCs, attributable to the presence of aluminum ions at the substitutional sites, forming shallow donor levels. The ferromagnetic behavior is understood on the basis of the nature of M (T) curve which is a manifestation of charge carrier concentration.

II. EXPERIMENTAL DETAILS

ZnO NCs capped with PVP were synthesized by the wet chemical route at room temperature.[13,15] X-ray diffraction (XRD) analysis was carried out on a Bruker AXS D8 advance powder x-ray diffractometer, with Cu K_α(1.5402 Å) as the incident radiation. Bandgap was determined by optical absorption studies using Perkin Elmer Lambda 950 UV-visible spectrophotometer. Photoluminescence (PL) and photoluminescence excitation (PLE) spectra of the NCs were measured on Perkin Elmer LS 55 spectrophotometer at room temperature and also at liquid nitrogen temperature (77 K). EPR measurements were performed at liquid nitrogen temperature (77 K) using Bruker EMX spectrometer operating at 9.1 GHz (X band). Magnetic measurements were carried out using superconducting quantum interference device (SQUID) magnetometer (Quantum Design, Inc.) in the temperature (T) range of 5 K to 300 K, and magnetic field (H) (–10) to 10

a)Electronic mail: shailajamahamuni@yahoo.co.in.

kOe. FC curves were recorded at magnetic field of 1 kOe. Elemental analysis was carried out using ICP-AES measurements (Spectra Arcos spectrometer). No magnetic impurity was detected in undoped as well as Al^{3+}-doped ZnO NCs.

III. RESULTS AND DISCUSSION

XRD patterns of PVP capped, undoped and Al^{3+}-doped ZnO NCs are shown in the inset of Fig. 1. Diffraction analysis reveals the characteristic wurtzite structure of ZnO NCs. The average size calculated from the width of XRD features by Scherrer formula[16] is 5.6 ± 0.3 nm. No secondary phase is observed in case of Al^{3+}-doped ZnO NCs. An ionic size of Al^{3+} (0.53 Å) being smaller than that of Zn^{2+} (0.72 Å),[13] aluminum ions occupy the substitutional site in ZnO without distorting the lattice. Figure 1 depicts room temperature optical absorption spectra of undoped and Al^{3+}-doped ZnO NCs. Al concentration in precursor solution is varied from 1% to 7.5%. The excitonic feature for undoped ZnO NCs is observed at 351 nm. The resulting blueshift in the absorption feature is given in Table I and is attributed to Moss-Burstein type shift[13] (due to increase in carrier concentration). Monotonic blueshift in absorption edge with increase in Al doping indicates effect thereof on the electron energy levels due to the substitutional incorporation of Al^{3+} in ZnO.

PL measurements were carried out at room temperature as well as at 77 K using the excitation wavelength of 325 nm. Al^{3+}-doped ZnO NCs show (not given here) gradual quenching of excitonic luminescence associated with appearance of defect (due to oxygen vacancies) related luminescence. The quantum efficiency of undoped ZnO NCs is calculated with respect to laser dye, polypropyleneoxide (PPO) and is found to be about 2.4% and that of Al^{3+}-doped ZnO NCs is about 0.5%. Inferior quantum efficiency is indicative of defects present in ZnO NCs. Al-doping causes an increase in the defect density. Figures 2(a) and 2(b) show PLE spectra of ZnO and Al^{3+}-doped ZnO NCs at room temperature (RT) and low temperature (LT). Relatively sharp PLE feature is seen in case of undoped ZnO NCs. On the other hand, PLE features are rather broad in case of Al^{3+}-doped ZnO NCs. Additional hump in Al^{3+}-doped NCs

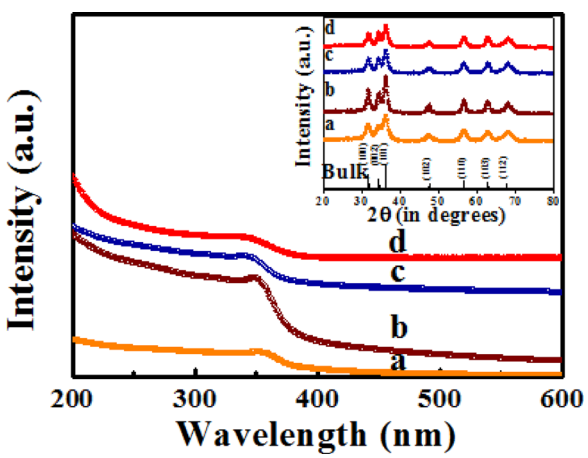

FIG. 1. (Color online) Optical absorption spectra of undoped and Al^{3+}-doped ZnO NCs. Inset: XRD pattern of (a) undoped, (b) 1% Al^{3+}-doped, (c) 2.5% Al^{3+}-doped, (d) 7.5% Al^{3+}-doped ZnO NCs.

TABLE I. Optical absorption features with varying Al precursor.

Al precursor in the reaction (%)	Amount of Al by ICP-AES (%)	Optical absorption (nm)	Optical absorption (eV)
0	0	351 (±2)	3.53 (±0.02)
1	0.12	346 (±2)	3.58 (±0.02)
2.5	0.22	343 (±1)	3.61 (±0.01)
7.5	1.4	338 (±1)	3.67 (±0.01)

at about 395 nm in PLE spectra is also observed.[13,17] At room temperature, PLE feature is located at 351 nm for ZnO NCs while it is located at 374 nm in case of Al^{3+}-doped ZnO NCs. On the other hand at 77 K, PLE feature appears at about 340 nm in both cases, indicating temperature activation of Al^{3+} ions.[18] This is a signature of the presence of large number of defects[13,17] in Al^{3+}-doped ZnO NCs.

EPR study is carried out at 77 K on undoped and Al^{3+}-doped ZnO NCs. Undoped ZnO NCs do not show EPR signal. A signal with g value 1.96 appears on incorporation of Al in ZnO NCs. Intensity of EPR signal increases with an increase in the amount of Al^{3+} ions in ZnO. EPR spectra of Al^{3+}-doped ZnO NCs with 7.5% doping level is presented in Fig. 3. In the present work, for ZnO NCs, no feature is observed in EPR. In undoped ZnO NCs such EPR signal is also observable[19–24] under special conditions. For instance, EPR spectra of undoped ZnO NCs dispersed in ethanol and toluene mixture (illuminated with Ar ion laser), were recorded by Whitaker *et al.*[24] The electron hole pair is generated due to the exposure to ultraviolet (UV) light. Hole

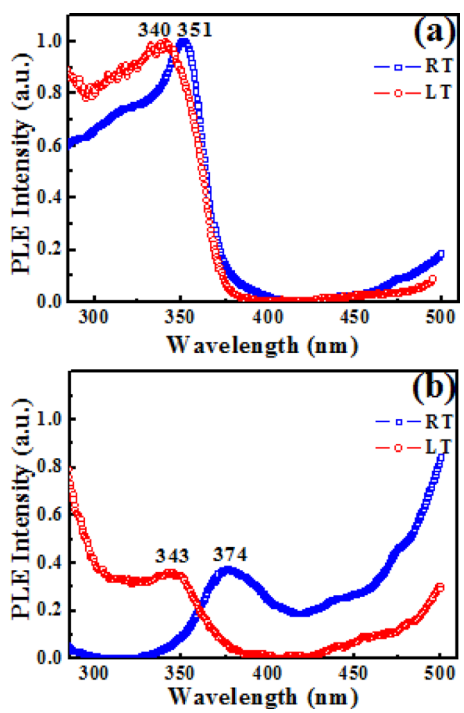

FIG. 2. (Color online) Photoluminescence excitation spectra recorded at wavelength of 530 nm in case of (a) undoped ZnO NCs and (b) Al^{3+}-doped ZnO NCs with doping level of 7.5% at room temperature (RT) as well as at 77 K (LT).

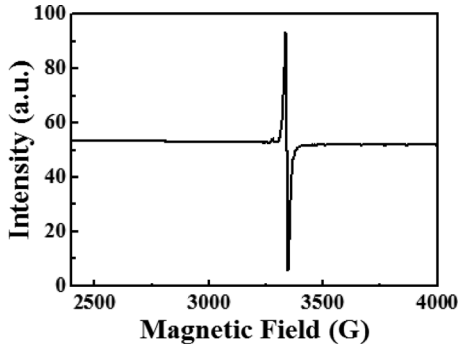

FIG. 3. EPR spectrum of Al^{3+}-doped ZnO NCs with doping level 7.5% in precursor solution.

remains trapped at the surface that eventually reacts with ethanol. EPR signal arises due to unreacted electron at $g = 1.96$. In the present case, clear EPR signal with $g = 1.96$ is observed in Al^{3+}-doped ZnO NCs. Similar EPR spectra of Al^{3+}-doped ZnO attributing $g = 1.96$ signal, to singly ionized oxygen vacancies[19,20,22] are reported. No UV light excitation was necessary to obtain EPR signal in these cases. Gradual increase in the number of point defects with Al content is visible in EPR spectra. Substitutional doping of Al^{3+} ions in ZnO NCs is unambiguously ascertained[21] to produce a shallow donor level with $g = 1.9595$. It is further contended that the most probable position of the substitutional Al shallow donor is at the center of the NC. We make use of this report to understand the ferromagnetic behavior of Al^{3+}-doped ZnO NCs.

Figure 4(a) exhibits the magnetization curve for undoped ZnO NCs at room temperature. Saturation magnetization (M_S) was observed to be 0.007 emu/g while coercivity (H_C) was observed to be 103 Oe. On cooling to 5 K, M_S and H_C increase up to 0.01 emu/g and, 140 Oe, respectively [Fig. 4(b)]. In this work, it is reasonable to assume the magnetization as superposition of two contributions: ferromagnetic/paramagnetic (M_{Fer})

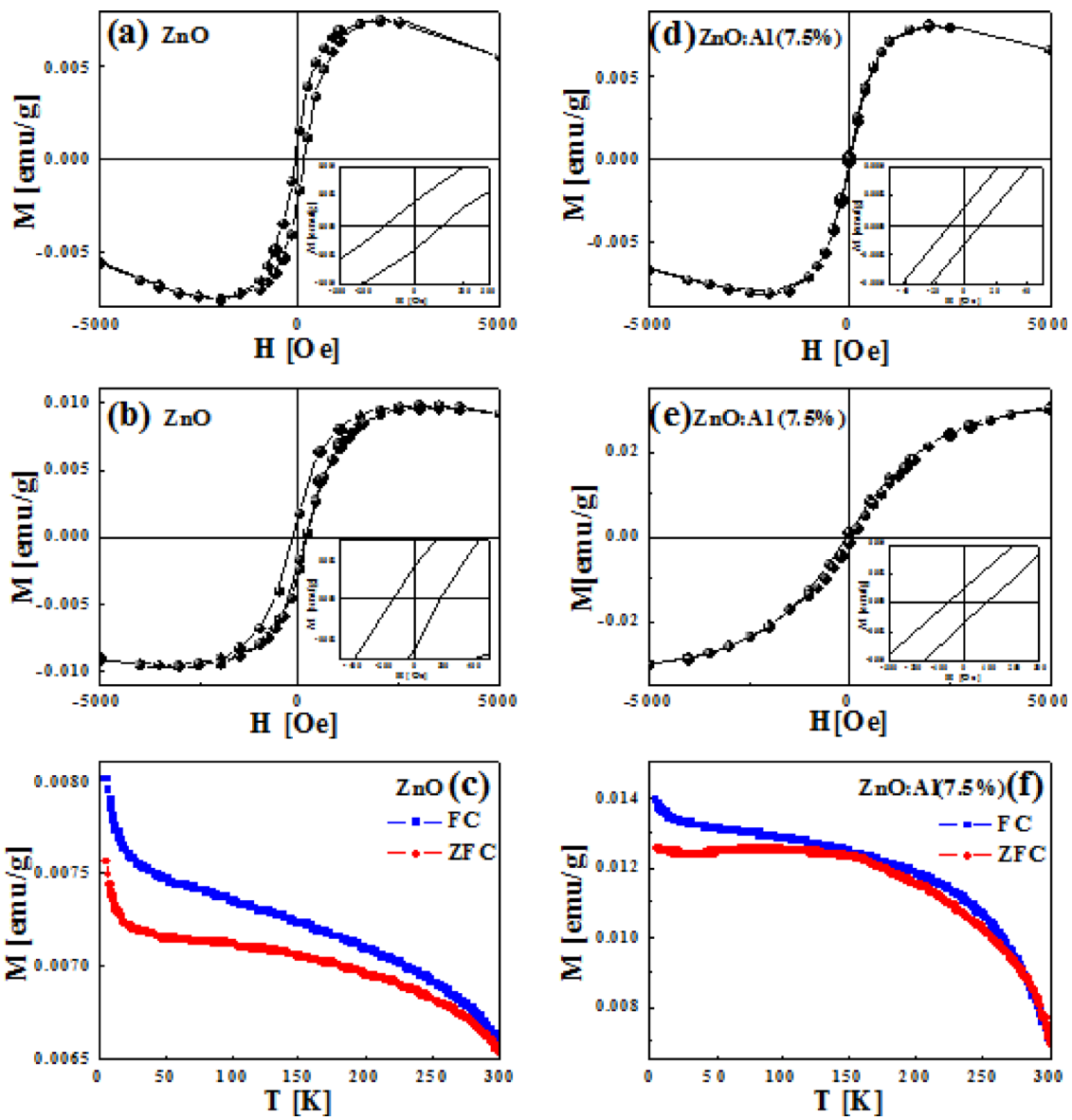

FIG. 4. (Color online) M vs H curves for (a) undoped ZnO at 300 K, (b) undoped ZnO at 5 K, (c) ZFC/FC curves of undoped ZnO NCs, (d) Al^{3+}-doped ZnO (7.5%) at 300 K, and (e) Al^{3+}-doped ZnO (7.5%) at 5 K, and (f) ZFC/FC curves of Al^{3+}-doped ZnO (7.5%) NCs in temperature range 5–300 K at applied field of 1 kOe. Insets show M (H) curves near $H = H_C$.

and diamagnetic (M_{Dia}) signals. It may be worthwhile to mention here that, in case of granular substances, diamagnetic susceptibility is observed[25,26] to be temperature dependent. Magnetoelastic effects alter the coupling and hence the diamagnetic susceptibility. In the present case, even though the apparent change in the diamagnetic contribution is vivid, subtraction of diamagnetic background does not significantly change the situation. Diamagnetic susceptibility [χ_{Dia} is of the order of 10^{-7} emu/g-Oe for all samples] is one order of magnitude lower than that of ferromagnetic susceptibility. The coercivity of the samples has been determined as a magnetic field where $M = M_{Fer}(T,H) + \chi_{Dia}H = 0$. Variation in diamagnetic contribution was checked carefully. The values thus obtained do not differ much from the experimentally deduced. Table II depicts saturation magnetization and coercivity values after correcting the diamagnetic contribution.

Earlier reports on ferromagnetic nanocrystal formation of otherwise diamagnetic materials indicate that the surface defects[2,3,6] as well as ligand induced defects[4,5,10] are instrumental. In case of uncapped ZnO NCs, M_S was observed[2] to be 6×10^{-4} emu/g. In the present study, NCs are capped with PVP. Further increase in M_S could be due to the defects generated by the capping agent. The bifurcation of ZFC/FC curves [Fig. 4(c)] shows the long range ferromagnetic ordering in undoped ZnO NCs.

As a result of doping Al^{3+} ions in ZnO NCs [Fig. 4(d)], M_S remains unaltered while coercivity reduces to about 10 Oe at room temperature. The experiments were repeated several times on freshly prepared Al^{3+}-doped ZnO NCs. The value of coercivity always reduced (with error of about 10%). At 5 K, the observed value of M_S is 0.032 emu/g and that of H_C is 76 Oe [Fig. 4(e)]. The reduction in coercivity of Al^{3+}-doped ZnO NCs compared to undoped ZnO NCs is notable. As reported by Orlinskii *et al.*,[21] Al^{3+} ions occupy substitutional position near the center of the NC (giving EPR signal with $g = 1.96$) and can also be located at the surface. The two different locations of Al^{3+} ions are instrumental for ferromagnetism in different ways. Surface defects are responsible for the ferromagnetic ordering in undoped ZnO as well as in Al^{3+}-doped ZnO NCs. Secondly, Al^{3+} ions incorporated in ZnO generate localized defect levels as projected by PLE and EPR observations. Consequently, small inner core of NC becomes ferromagnetic. Defect centers are known[1,10] to produce magnetic polarization localized in the lattice and is well documented. Such a ferromagnetic cluster formation is feasible in vicinity of Al^{3+} ion located near the center of ZnO NC. It is worthwhile to note that ZFC/FC curve of Al^{3+}-doped ZnO nanocrystal [Fig. 4(f)] shows ferromagnetic nature. An increase in the magnetizations at low temperatures is due to the presence of paramagnetic ions.[27] Notable fact is the convex nature of M(T) curves in case of Al^{3+}-doped ZnO NCs. As discussed earlier, Al^{3+} ions reveal thermal activation. As temperature increases, Al^{3+} ions liberate charge carriers, and in turn, that is reflected in the shape of spontaneous magnetization as a function of temperature curves. In fact, using different theoretical models, it is ascertained[28,29] that semiconductors with localized charge carriers depict concave M(T) curve and the ferromagnetic interaction is triggered by percolation of bound magnetic polarons (BMP). On the other hand, at higher charge carrier concentration, the interactions are carrier mediated and reflected in the convex M(T) curve. A fingerprint analysis of magnetic interactions is thus possible from the shape of M(T) curves. An enhanced convexity in M(T) curve in case of Al^{3+}-doped ZnO NCs is a signature of ferromagnetic ordering mediated via charge carriers. Earlier, we have reported[13] an increase in the charge carrier concentration in Al^{3+}-doped ZnO NCs prepared by different methods. At low carrier concentration level in undoped ZnO NCs, M(T) curve exhibits outwardly concave magnetization behavior wherein BMPs trigger the long range ferromagnetic order.

Possibility of Al^{3+} ions located at or near surface cannot be ruled out. Al^{3+} ions spatially located near or on the surface of NCs (those are not EPR sensitive but quench excitonic PL) appear to cause adverse effects on ferromagnetic ordering. The surface defects, mostly oxygen vacancies, do contribute to ferromagnetism of undoped ZnO NCs. The surface defects are modulated by Al^{3+} ions in doped ZnO NCs. Subsequently, M_S is not improved in Al^{3+}-doped ZnO NCs while room temperature coercivity is reduced. The present work suggests that Al^{3+} ions located beneath the surface are, in fact, destroying percolating BMPs responsible for long range ordering. Similar behavior is observed[14] in case of V-doped ZnO.

TABLE II. Saturation magnetization and coercivity values of ZnO and ZnO:Al NCs.

	300 K		5 K	
Sample	M_S(emu/g)	H_C(Oe)	M_S(emu/g)	H_C(Oe)
ZnO	0.007	103	0.01	140
ZnO:Al (7.5%)	0.008	10	0.032	76

IV. CONCLUSIONS

To summarize, defects responsible for ferromagnetic ordering in Al^{3+}-doped ZnO NCs are identified by EPR spectroscopy. PVP capped, undoped ZnO NCs are weakly ferromagnetic at room temperature. Optical studies indicate presence of defects in NCs. The mechanism of ferromagnetism is altogether different in the case of ZnO NCs and Al^{3+}-doped ZnO NCs. In case of Al^{3+}-doped ZnO NCs, coercivity is substantially reduced, while saturation magnetization remains invariant at room temperature. M(T) curve in case of Al^{3+}-doped ZnO NCs is outwardly convex while in case of undoped ZnO NCs it is concave. RTFM, in case of undoped ZnO NCs, is understandable in terms of BMP. Al^{3+}-induced defects with $g = 1.96$ are vivid from EPR spectra. Thereby, one may conclude that the resultant ferromagnetism has two components. Defects located at the surface induce ferromagnetism. Furthermore, the magnetic moments associated with the defects formed due to Al^{3+} ions also yield ferromagnetism. The exchange interaction mechanism in Al^{3+}-doped ZnO NCs appears to be charge carrier mediated.

ACKNOWLEDGMENTS

This work is supported by Department of Science and Technology, India, the Research Opportunity Award from Research Corporation (RA-0357), and by the Office of Basic Energy Sciences, Material Sciences Division of the U. S. Department of Energy (Contract No. DE-FGP2-06ER46291). D.Y.I. would like to thank CSIR for the financial support. Authors are grateful for the funding by the DST Nano-initiative and the U.G.C. under University with Potential for Excellence for the characterization facilities. ICP-AES and EPR measurements were carried out at S.A.I.F., IIT, Mumbai.

[1]M. Venkatesan, C. B. Fitzgerald, and J. M. D. Coey, Nature **430**, 630 (2004).
[2]A. Sundaresan, R. Bhargavi, N. Rangarajan, U. Siddesh, and C. N. R. Rao, Phys. Rev. B **74**, 161306(R) (2006).
[3]S. Bannerjee, M. Mandal, N. Gayathri, and M. Sardar, Appl. Phys. Lett. **91**, 182501 (2007).
[4]P. Crespo, R. Litrán, T. C. Rojas, M. Multigner, J. M. de la Fuente, J. C. Sánchez-López, M. A. García, A. Hernando, S. Penadés, and A. Fernández, Phys. Rev. Lett. **93**, 087204 (2004).
[5]M. A. Garcia, J. M. Merino, P. E. Fernández Pinel, A. Quesada, J. de la Venta, M. L. Ruíz González, G. R. Castro, P. Crespo, J. Llopis, J. M. González-Calbet, and A. Hernando, Nano Lett. **7**, 1489 (2007).
[6]K. Potzger, S. Zhou, J. Grenzer, M. Helm, and J. Fassbender, Appl. Phys. Lett. **92**, 182504 (2008).
[7]C. Madhu, A. Sundaresan, and C. N. R. Rao, Phys. Rev. B **77**, 201306(R) (2008).
[8]H. Pan, J. B. Yi, L. Shen, R. Q. Wu, J. H. Yang, J. Y. Lin, Y. P. Feng, J. Ding, L. H. Van, and J. H. Yin, Phys. Rev. Lett. **99**, 127201 (2007).
[9]K. W. Liu, M. Sakurai, and M. Aono, J. Appl. Phys. **108**, 043516 (2010).
[10]D. Y. Inamdar, A. D. Lad, A. K. Pathak, I. Dubenko, N. Ali, and S. Mahamuni, J. Phys. Chem. C **114**, 1451 (2010).
[11]D. Gao, J. Zhang, G. Yang, J. Zhang, Z. Shi, J. Qi, Z. Zhang, and D. Xue, J. Phys. Chem. C **114**, 13477 (2010).
[12]K. Yang, R. Wu, L. Shen, Y. P. Feng, Y. Dai, and B. Huang, Phys. Rev. B **81**, 125211 (2010).
[13]P. Kadam, C. Agashe, and S. Mahamuni, J. Appl. Phys. **104**, 103501 (2008).
[14]S. H. Liu, H. S. Hsu, G. Venkataiah, X. Qi, C. R. Lin, J. F. Lee, K. S. Liang, and J. C. A. Huang, Appl. Phys. Lett. **96**, 262504 (2010).
[15]L. Guo, S. Yang, C. Yang, P. Yu, J. Wang, W. Ge, and G. K. L. Wong, Chem. Mater. **12**, 2268 (2000).
[16]B. D. Cullity, *Elements of X-ray Diffraction* (Addison Wesley, Reading, MA, 1978).
[17]T. B. Hur, Y. H. Hwang, and H. K. Kim, J. Appl. Phys. **96**, 1507 (2004).
[18]H. P. He, H. P. Tang, Z. Z. Ye, L. P. Zhu, B. H. Zhao, L. Wang, and X. H. Li, Appl. Phys. Lett. **90**, 023104 (2007).
[19]P. H. Kasai, Phys. Rev. **130**, 989 (1963).
[20]C. Gonzalez, D. Block, R. T. Cox, and A. Hervi, J. Cryst. Growth **59**, 357 (1982).
[21]S. B. Orlinskii, J. Schmidt, P. G. Baranov, V. Lorrmann, I. Riedel, D. Rauh, and V. Dyakonov, Phys. Rev. B **77**, 115334 (2008).
[22]K. Vanheusden, C. H. Seager, W. L. Warren, D. R. Tallant, and J. A. Voigt, Appl. Phys. Lett. **68**, 403 (1996).
[23]B. K. Meyer, H. Alves, D. M. Hofmann, W. Kriegseis, D. Forster, F. Bertram, J. Christen, A. Hoffmann, M. Straßburg, M. Dworzak, U. Haboeck, and A. V. Rodina, Phys. Stat. Sol. (b) **241**, 231 (2004).
[24]K. M. Whitaker, S. T. Ochsenbein, V. Z. Polinger, and D. R. Gamelin, J. Phys. Chem. C **112**, 14331 (2008).
[25]R. Hajndl, J. Sanders, H. Srikanth, and N. J. Dudney, J. Appl. Phys. **93**, 7999 (2003).
[26]R. M. Candea, C. M. Gee, S. J. Hudgens, and M. Kastner, Phys. Rev. B **16**, 2657 (1977).
[27]G. Clavel, N. Pinna, and D. Zitoun, Phys. Stat. Sol. (a) **204**, 118 (2007).
[28]M. J. Calderon and S. Das Sarma, Ann. Phys. **322**, 2618 (2007).
[29]S. Das Sarma, E. H. Hwang, and A. Kaminski, Phys. Rev. B **67**, 155201 (2003).